TRANSACTIONS OF THE INSTITUTE OF FLUID-FLOW MACHINERY

No. 136, 2017, 65–76

Kamil Banaś* and Janusz Badur

On an approach to the thermo-elasto-plastic failure based on the Burzynski criterion

Institute of Fluid-Flow Machinery, Polish Academy of Sciences, Fiszera 14, 80-231 Gdańsk, Poland

Abstract

In this paper the comparison of material effort models: the classic Huber-Mises-Hencky approach and the Burzynski condition was presented. Burzynski yield condition is pressure sensitive and naturally takes into account the strength differential effect, which has been observed in nickel-base super alloys such as Inconel 718. Investigation was performed during thermal-fluid-structure interaction analysis of a power turbine guide vane of turbine helicopter engine PZL-10W. Firstly, computational fluid dynamics conjugate heat transfer analysis was carried out, then stress analysis was performed with boundary conditions obtained via computational fluid dynamics analysis. During stress analysis, two mentioned above equivalent stress definitions were applied and difference in material effort modelling by them was shown.

Keywords: Burzynski stress; Thermal-FSI; Conjugate heat transfer; Thermal stresses; Turbine guide vane

1 Introduction

The inlet temperature plays an essential role in the performance of gas and steam turbines, where cyclic thermo-elasto-plasticity and high-temperature creep may interact and contribute to failure [1–3]. Much effort has been made to develop methods to predict the temperature, thermal stresses, and associated lifetime of critical components in the aerospace and power generation industries [4–9]. Accurate prediction and assessment of the material effort (the risk of fracture)

*Corresponding author. E-mail address: kbanas@imp.gda.pl

are important for these processes.

According to Włodzimierz Burzyński:

> *Generally, under the notion: material effort we understand the physical state of a body, comprehended in the sense of elasticity or plasticity or material strength, and generated by a system of stresses, and related with them strains, in the body* [10].

In the elastic state, an equivalent stress defined by an assumed hypothesis is commonly used as a measure of material effort during the design process. The stresses should be kept within an allowable limit.

An overwhelming majority of structural analyses use the classical Huber-Mises-Hencky (HMH) J_2 plasticity theory to define equivalent stresses and describe the plastic response of metallic alloys:

$$F(J_2) = \sqrt{3J_2} \; - \; \sigma_Y^T \; , \tag{1}$$

where J_2 is the second invariant of the deviatoric stress tensor. However, it was shown experimentally [11–14] and numerically that the HMH yield condition is insufficient to simulate the response of metals that exhibit different values of yield stresses in tension σ_Y^T and compression σ_Y^C, which is known as the strength differential (SD) effect [15–18].

The SD effect is characterized by the SD parameter

$$k = \frac{\sigma_Y^C}{\sigma_Y^T} \; . \tag{2}$$

The effect has been observed in many iron-based metals, such as 4310, 4330, maraging, and HY80 steels [11–12], as well as titanium, aluminium 2024-T351 [15], magnesium, and nickel-base super alloys such as Inconel 718 [19]. The SD effect for isotropic materials is related to the pressure sensitivity of the yield points, the influence of the Lode angle on the yield points, or both [20].

Hu discovered the influence of pressure on the yielding of aluminium alloy in the 1950s [21–22]. In the 1960s, Hu performed pressurized tension tests on Nittany No. 2 brass and found that hydrostatic pressure affected the yield strength [23]. In the 1970s and early 1980s, Richmond, Spitzig, and Sober [11–14] studied the effects of hydrostatic pressure (up to 1100 MPa) on the plasticity for four steels (4310, 4330, maraging steel, and HY80) and grade 1100 aluminum. The steels showed the SD effect, and hydrostatic pressure influenced their yield strengths and stress flow. Nevertheless, there was no influence on their work-hardening characteristics. The aluminium alloy did not exhibit the SD effect, and pressure influenced the stress flow and work-hardening characteristics, which shows the independence of SD effect and pressure sensitivity in general. The yield function

developed by Richmond was identical to the one proposed originally in 1928 by Burzynski [24–25] and in the 1950s by Drucker and Prager [26]:

$$F(I_1, J_2) = aI_1 + \sqrt{3J_2} - d\,, \tag{3}$$

where I_1 is the the first invariant of stress tensor, d is the modified yield strength in the absence of the mean stress, and a is a material constant related to the theoretical cohesive strength of the material.

It is well documented that the large hydrostatic stresses that develop in sharply notched or cracked geometries can exceed 1000 MPa [20]. Wilson [15] conducted experiments and nonlinear finite element analyses of notched round bars (NRBs) made of aluminium 2024-T351, which shows the SD effect. He modeled the loading of an NRB to failure using the HMH and Drucker-Prager yield functions. The HMH results overestimated the experimental load-displacement curves, while the Drucker-Prager FEA results essentially matched the experimental data.

The experimental observations have shown the effect of Lode angle (or the third deviatoric stress invariant) on the yield surface of materials that show the SD effect. The effect of the Lode angle appears particularly apparent during shear processes place. This was proven experimentally and numerically by Bai and Wierzbicki [17]. They tested NRBs and flat grooved specimens made of aluminium 2024-T351. The flat grooved specimen had the same range of stress triaxiality as the NRB, but the corresponding values of the Lode angle parameter were different [17]. This feature gives a direct way to see the effect of Lode angle parameter on metal plasticity. Bai and Wierzbicki evaluated the $I_1J_2J_3$ yield condition. They numerically proved that correction for the pressure effect is not enough, and the Lode angle parameter effect should also be taken into account in the formulation of the yield condition.

Iyer and Lissenden also examined the influence of the third invariant of stress deviator tensor on the yielding of metals, which exibit the SD effect [16]. They tested aged Inconel 718 at an elevated temperature of 650 °C. They considered nonproportional loading of hollow tubes, such as a shear strain followed by an axial strain. The J_2J_3 class models were found to agree the best with the experimental results. However, the J_2J_3 and $I_1J_2J_3$ class models were both able to predict the stress and strain response from the six biaxial load paths almost equally well.

Lewandowski conducted hydrostatic pressure tests at pressures of up to 450 MPa on Inconel 718 at room temperature [27]. These tests indicated that hydrostatic pressure does not significantly affect the plastic flow. Between 0.1 and 450 MPa, the compression yield strength decreases by around 28 MPa [27]. Pressures of up to 450 MPa cover the range of internal pressure produced during Iyer and Lissenden's tests [16]. However, the internal pressure in an actual geometry can

exceed this value (Tab. 1).

For hexagonal close packed materials, twinning and texture evolution contribute to the SD effect [28–29]. As these metals are pressure insensitive, the dependence of the yield condition on the first stress invariant should be neglected, and the effect of the third stress deviator invariant J_3 becomes important [28–29].

In our work, we consider the paraboloid case of Burzynski yield condition [18,24,25,30]

$$F(\sigma_m, \sigma_e, \sigma_Y^T, k) = \frac{1}{2k}\left[3(k-1)\sigma_m + \sqrt{9(k-1)^2\sigma_m^2 + 4k\sigma_e^2}\right] - \sigma_Y^T \,, \qquad (4)$$

which is pressure sensitive and naturally takes into account the SD effect. Here σ_m represents hydrostatic stress and σ_e is the HMH stress. The material effort of materials which reveal strength differential effect are described more accurately by the Burzynski model than the Huber-Mises-Hencky approach, as shown on the example of Inconel 718 [18], which is widely used in aerospace industry. In this work, comparison of equivalent stresses obtained by applying the Burzynski parabolic model and the classic HMH definition was performed. Investigation was carried out based on thermal-fluid-structure interaction (FSI) analysis of a power turbine guide vane of a turbine helicopter engine PZL-10W made of Inconel 738. The elastic range was considered. The vane is uncooled, but we included cooling of rotor disc and cooling of casing, which locally decreases temperature in structure, which causes high temperature gradient and consequently leads to thermal stresses. Firstly, computational fluid dynamics (CFD) conjugate heat transfer analysis was carried out using Ansys Fluent software. Then stress analysis by Ansys Mechanical was performed with boundary conditions obtained during CFD analysis.

2 Burzynski material effort model

Burzynski presented an energetic hypothesis for materials that show the SD effect. He proposed defining the limit of elastic range as a sum of u^D, which is the specific elastic distortional energy, and u^A, which is a part of specific elastic volumetric energy [24,25]:

$$u^D + \eta u^A = K \,, \qquad (5)$$

where the parameter $\eta = \omega + \frac{\delta}{3\sigma_m}$ depends on material parameters ω, δ, which represent the contribution of specific elastic volumetric energy influenced by the hydrostatic stress $\sigma_m = \frac{1}{3}\sigma_{ii}$. The constant K denotes the specific elastic energy at the yield point. Burzynski evaluated the parameters K, ω, and δ using quantities commonly evaluated during material test, σ_Y^T, σ_Y^C, and σ_Y^S which denote the yield limit in tension, compression and shear tests respectively. This leads to the

following form [18,24,25,30]:

$$\frac{\sigma_Y^C \sigma_Y^T}{(3\sigma_Y^S)^2}\sigma_e^2 + \left[9 - \frac{3\sigma_Y^C \sigma_Y^T}{(\sigma_Y^S)^2}\right]\sigma_m^2 + 3(\sigma_Y^C - \sigma_Y^T)\sigma_m - \sigma_Y^C \sigma_Y^T = 0\,, \tag{6}$$

where $\sigma_e = \sigma_{HMH}$ denotes the HMH stress. The introduction of harmonic mean relation between material constants: $\sigma_Y^S\sqrt{3} = \frac{2\sigma_Y^T\sigma_Y^C}{\sigma_Y^T+\sigma_Y^C}$ leads to the relation that was independently evaluated by Drucker-Prager [18,24,26,30]:

$$\sigma_e + 3\frac{\sigma_Y^C - \sigma_Y^T}{\sigma_Y^C + \sigma_Y^T}\sigma_m - 2\frac{\sigma_Y^C \sigma_Y^T}{\sigma_Y^C + \sigma_Y^T} \;=\; 0\,. \tag{7}$$

However, the assumption of a geometric mean $\sigma_Y^S\sqrt{3} = \sqrt{\sigma_Y^T\sigma_Y^C}$ leads to the Burzynski-Torre parabolic model [18,24,30,31]:

$$\sigma_e^2 + 3\left(\sigma_Y^C - \sigma_Y^T\right)\sigma_m - \sigma_Y^C \sigma_Y^T = 0\,, \tag{8}$$

which after introducing the SD parameter , Eq. (2), can be rewritten as [18]

$$\sigma_e^2 + 3\left(k-1\right)\sigma_m\sigma_Y^T - \left(\sigma_Y^T\right)^2 k = 0\,. \tag{9}$$

After solving with respect to σ_Y^T and extracting the positive root, final form of the Burzynski yield condition is obtained [18]

$$F(\sigma_m, \sigma_e, \sigma_Y^T) = \frac{1}{2k}\left[3(k-1)\sigma_m + \sqrt{9(k-1)^2\sigma_m^2 + 4k\sigma_e^2}\right] - \sigma_Y^T = 0\,. \tag{10}$$

The Burzynski equivalent stress has the following form:

$$\sigma_B \;=\; \frac{1}{2k}\left[3(k-1)\sigma_m + \sqrt{9(k-1)^2\sigma_m^2 + 4k\sigma_e^2}\right]\,. \tag{11}$$

3 Thermal-FSI analysis

Considering heat transfer in structural parts, temperature distribution is not our final aim. We would like to know how temperature affects our structure. Thermal-FSI analysis offers an excellent approach to this purpose. The power turbine guide vane (Fig. 1) of helicopter engine PZL-10W is considered.The structure is relatively stiff, so that deformations do not influence the heat transfer. Taking this fact into account we considered one-way thermal-FSI analysis (Fig. 2). In first step we investigated conjugate heat transfer analysis to obtain temperature field in solid bodies and pressure acting on vane. Then, stress analysis with boundary conditions obtained during CFD analysis was performed.

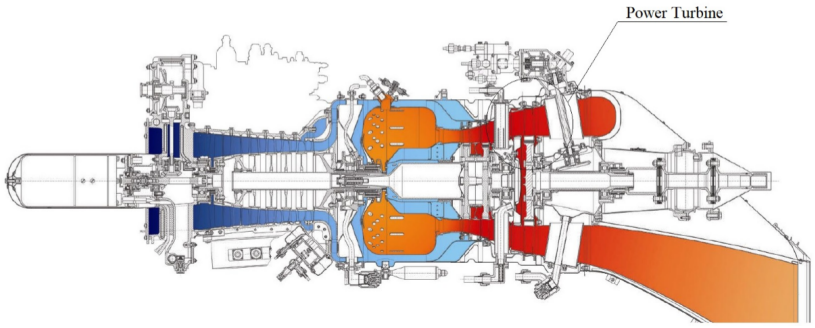

Figure 1. PZL-10W – gerneral view with pointed out power turbine.

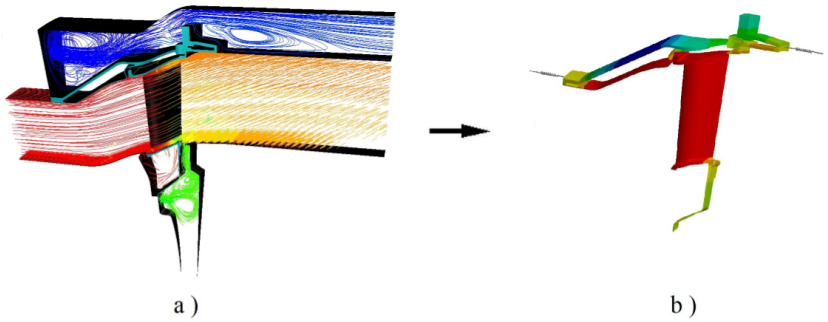

Figure 2. One way thermal-FSI analysis scheme: a) computation fluid dynamics (CFD) – streamline shading by temperature b) computation solid dynamics (CSD) – thermal boundary conditions

3.1 Conjugate heat transfer analysis

Modelled domain consists of 4 fluid domains and 4 solid domains (Fig. 3a). Main fluid domain was modelled as flue gas assuming compressible, calorically imperfect gas, therefore specific heat and other properties vary with temperature. We assumed single component gas for which we evaluated average properties from the relationship for mixtures. We assumed flue gas consists of the following mole fractions: 75.8% N_2, 16.8% O_2, 4.1% H_2O, 3.3% CO_2. Average viscosity was obtained from Sutherland's relation for mixtures [32], thermal conductivity from the Chapman-Enskog relation. Specific heat for each component was obtained from polynomial function than average quantity was obtained taking volume fraction into account. Fluid cooling casing was modelled as air with properties which vary with temperature. Solids properties were modelled depending on temperature.

Relatively fine unstructured mesh was created, it consists of 3 200 000 polyhedral elements with conformal solid-fluid and solid-solid interfaces (Fig. 3b).

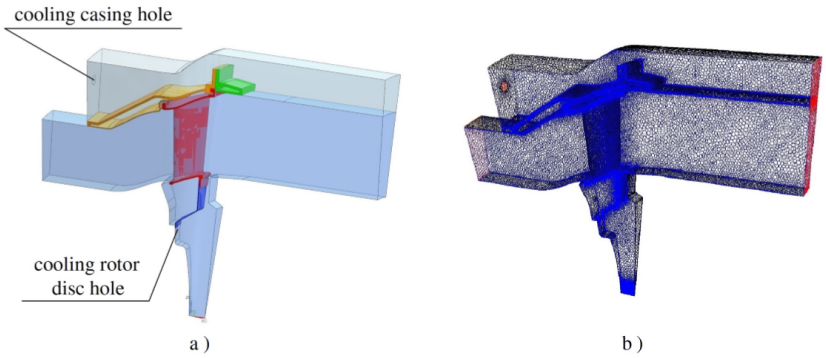

Figure 3. CFD models: a) computer aid design (CAD) picture b) finite volume discretization.

In order to capture the effects in momentum and thermal boundary layers the low-Reynolds eddy-viscosity SST γ-Re$_\theta$. Transition turbulence model [33,34] was used and mesh was build based on dimensionless parameter $y^+ \approx 1$ near walls.

The disc is cooled by air taken from the compressor outlet, while casing is cooled by air delivered from the environment. We assumed that the mass flow rate of fluid cooling the disc is 1% of mass flow rate of the main flow.

3.2 Stress analysis

After the temperature field and pressure distribution had been obtained via CFD, we used them as boundary conditions (Fig. 4) during stress analysis.

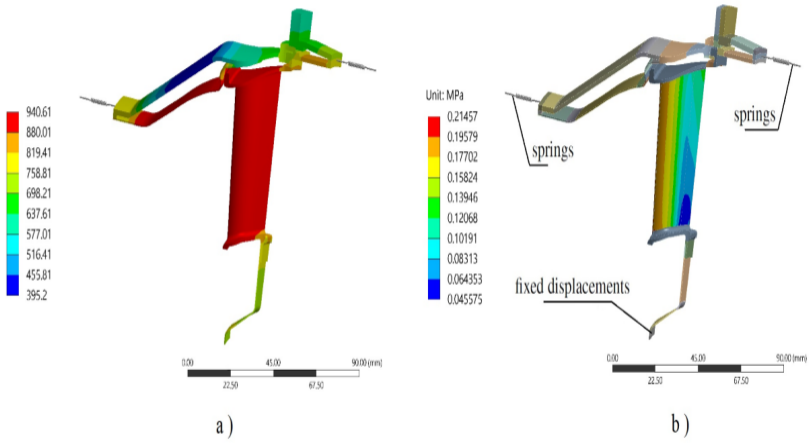

Figure 4. FEM boundary conditions: a) thermal b) mechanical.

For stress analysis we applied the isoparametric elements with quadratic shape function. Because the guide vane is connected with casing by joint studs, we modelled connection between them by constraint equation which fix rotation with respect to the axis of rotation. Owing to this constraint, a torque between vane and casing was transferred. Other connections were modelled by frictional contact with 0.2 friction coefficients. The model had got fixed displacements in bottom part due to connection with essentially stiffer body in that place. Instead of the fixed displacements on casing we applied springs with longitudinal and torsional stiffnesses (Fig. 4b). Those stiffnesses were obtained by additional analyses. Radial direction of casing is free.

Due to the lack of experiment data of compression yield strength for Inconel 738 lc we assumed strength differential parameter equal $k = 1.10$.

4 Results of thermal-FSI simulations

Figure 5 presents the values of temperature at characteristic points, which represent maximum temperature at stagnation point and influence of cooling casing and rotor disk. We can notice high gradient of temperature causing by cooling casing and rotor disk.

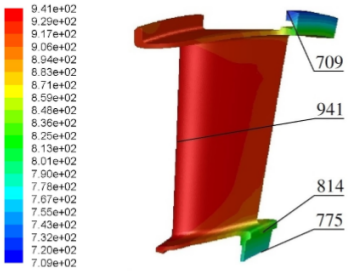

Figure 5. Values of temperature in kelvins at characteristic points.

The Burzynski and the HMH criterions were compared at a few critical points on vane presented on Fig. 6. Values of equivalent stresses, based on the Huber-Mises-Hencky and the Burzynski material effort definition, obtained at critical points are presented in Tab. 1. Table 1 shows us the discrepancies between material effort models are rather huge. The biggest difference is for maximum level of stress and it is 66 MPa, which is around 11% relative error. Maximum relative error occurs for S3 point and it is 12%. We can notice, that the Huber-Mises-Hencky equivalent stresses are higher than stresses according to the Burzynski definition. If we compare these two definitions, we can evaluate relations Eq. (12),

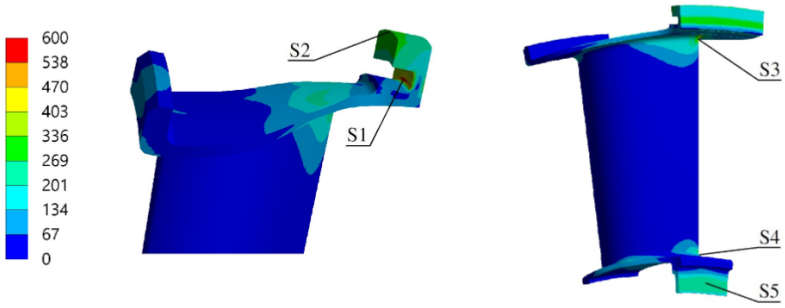

Figure 6. Schematically showed places of measured stress level.

Table 1. Equivalent stress: the Burzynski, σ_B, and the Huber-Mises-Hencky, σ_e, at different points

Equivalent stress [MPa]					
Point	S1	S2	S3	S4	S5
Burzynski	534	317	376	188	236
Huber-Mises-Hencky	600	317	425	208	247

which show that, when $\sigma_e < 3\sigma_m$, then the Burzynski stress is higher than the Huber-Mises-Hencky stress:

$$\begin{aligned} \sigma_e < 3\sigma_m \quad &\rightarrow \quad \sigma_B > \sigma_e \ , \\ \sigma_e > 3\sigma_m \quad &\rightarrow \quad \sigma_B < \sigma_e \ . \end{aligned} \tag{12}$$

An example of such a place on considered vane, where the Burzynski equivalent stress exceeded the Huber-Mises-Hencky stress, is shown in Fig. 7.

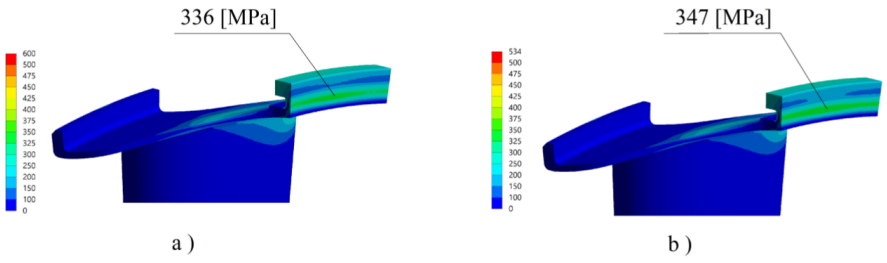

Figure 7. Equivalent stress: a) Huber-Mises-Hencky, b) Burzynski.

5 Conclusions

Thermal-FSI analysis of power turbine guide vane of turbine engine was performed. The vane is uncooled, but cooling of rotor disc and cooling of casing were included. Applying cooling decreased locally temperature in the vane, which in consequence caused higher temperature gradients in structure and finally induced high thermal stresses. Firstly, conjugate heat transfer analysis was carried out. Then stress analysis was performed with boundary condition obtained via CFD. The HMH material effort models was compared with the paraboloid case of Burzynski definition. The discrepancies between material effort models were rather huge. The biggest difference 66 MPa occurred for maximum level of stresses which appeared in top part of the vane, where Burzynski stress was 534 MPa, while HMH 600 MPa, so 66 MPa is around 11% relative error. Maximum relative error 12% occurred in airfoil and shroud connection place, from trailing edge side. Level of stresses there were 376 MPa for Burzynski definition and 425 MPa for HMH approach, so difference in that place was 49 MPa. For the most interesting places Burzynski stresses were smaller than HMH stresses. However, evaluated relations Eq. (12) show that, when $\sigma_e < 3\sigma_m$, then the Burzynski stress is higher than the HMH stress. An example of such a place on the vane was shown, where Burzynski stress was 347 MPa, while stress evaluated by HMH model was 336 MPa.

Obtained results showed the huge influence of the SD effect on the equivalent stresses in a highly loaded structure. Maximally, 12% discrepancy between criterions was obtained and maximum stresses differed by 11%, which is significant both from static and life time points of view.

Received in March 2017

References

[1] Badur J., Karcz M., Kucharski R., Wisniewski A., Kekana M.: *Coupled modelling of the cooling processes and the induced thermo-corrosive fatigue within a gas turbine.* Cracow TU, 2003, 19–30.

[2] Badur J., Ziółkowski P., Sławiński D., Kornet S.: *An approach for estimation of water wall degradation within pulverized-coal boilers.* Energy **92**(2015), 142–152.

[3] Banaszkiewicz M.: *Numerical investigation of creep behaviour of high-temperature steam turbine components.* Trans. Inst. Fluid-Flow Mach. **124**(2012), 5–15.

[4] Banaś K., Badur J.: *Influence of turbulence RANS models on heat transfer coefficients and stress distribution during thermal-FSI analysis of power turbine guide vane of helicopter turbine engine PZL-10W taking into account convergence of heat flux.* Progress in Computational Fluid Dynamics, 2017.

[5] Banaszkiewicz M.: *Online determination of transient thermal stresses in critical steam turbine components using a two-step algorithm.* J. Therm. Stresses **6**(2017), 690–703.

[6] Banaszkiewicz M.: *On-line monitoring and control of thermal stresses in steam turbine rotors.* Appl. Therm. Eng. **94**(2016), 763–776.

[7] Staroselsky A., Martin T.J., Cassenti B.: *Transient thermal analysis and viscoplastic damage model for life prediction of turbine components.* J. Eng. Gas Turb. Power **137**(2015), 042501.

[8] Taler J., Weglowski B., Sobota T., Jaremkiewicz M., Taler D.: *Inverse Space Marching Method for Determining Temperature and Stress Distributions in Pressure Components.* In: Development in Heat Transfer (M.A.D.S. Bernardes, Ed.), In Tech, Rijeka 2011, ISBN: 978-953-307-569-3.

[9] Duda P.: *Inverse Method for stress monitoring in pressure components of steam generators.* In: Proc. 17th Int. Conf. on Structural Mechanics in Reactor Technology, 2003.

[10] Burzyński W.: *Selected passages from Włodzimierz Burzynski's doctoral dissertation: Study of material effort hypotheses.* Eng. Trans. **57**(2009), 185–215.

[11] Spitzig W.A., Sober R.J, Richmond O.: *Pressure dependence of yielding and associated volume expansion in tempered martensite.* Acta Metallurgica **7**(1975), 885–893.

[12] Spitzig W.A., Sober R.J., Richmond O.: *The Effect of Hydrostatic Pressure on the Deformation Behavior of Maraging and HY-80 Steels and its Implications for Plasticity Theory.* Metall. Trans. **11**(1976), 377–386.

[13] Richmond O., Spitzig W.A.: *Pressure dependence and dilatancy of plastic flow.* In: Proc. IUTAM Conf., North-Holland, 1980, 377–386.

[14] Spitzig W.A., Richmond O.: *The effect of pressure on the flow stress of metals.* Acta Metallurgica **32**(1984), 457-463.

[15] Wilson C.D.: *A critical reexamination of classical metal plasticity.* J. Appl Mech. **69**(2002), 63–68.

[16] Iyer S.K., Lissenden C.J.: *Multiaxial constitutive model accounting for the strength-differential in Inconel 718.* Int. J. Plasticity **19**(2003), 2055–2081.

[17] Bai Y., Wierzbicki T.: *A new model of metal plasticity and fracture with pressure and Lode dependence.* Int. J. Plast. **24**(2008), 1071–1096.

[18] Vadillo G., Fernandez-Saez J., Pecherski R.B.: *Some applications of Burzynski yield condition in metal plasticity.* Mat. Des. **32**(2011), 628–635.

[19] Gil C.M., Lissenden C.J., Lerch B.A.: *Yield of Inconel 718 by axial-torsional loading at temperature up to 649 C.* J. Test. Eval. **27**(1999), 327–336.

[20] Pecherski R.B., Fras T., Nowak M.: *Inelastic flow and failure of metallic solids.* CISM Lectures, Udine, 2012.

[21] Marin J., Hu L.W.: *On the validity of assumptions made in theories of plastic flow for metals.* Trans. ASME **75**(1953), 1181–1190.

[22] Hu L.W., Bratt J.F.: *Effect of tensile plastic deformation on yield condition.* J. Appl. Mech. **25**(1958), 411.

[23] Hu L.W.: *Plastic Stress-Strain Relations and Hydrostatic Stress.* In: Proc. 2nd Symp. on Naval Structural Mechanics: Plasticity, Brown University, Rhode Island 1960, 194–201.

[24] Burzynski W.: *Theoretical foundations of the hypotheses of material effort.* Czasopismo Techniczne **47**(1929), 1–41.

[25] Burzynski W.: *Ueber die Anstrengungshypothesen.* Schweiz Bauzeitung **94**(1982), 259–262.

[26] Drucker D.C., Prager W.: *Soil mechanics and plastic analysis for limit design.* Quart. Appl. Math. **10**(1952), 157–165.

[27] Lewandowski J.J., Wesseling P., Prabhu N.S., Larose J., Lerch B.A.: *Strength differential measurements in IN 718: Effects of superimposed pressure.* Metall. Mater. Trans. A **8**(2003), 1736–1739.

[28] Raniecki B., Mroz Z.: *Yield or martensitic phase transformation conditions and dissipation functions for isotropic, pressure-insensitive alloys exhibiting SD effect.* Acta Mechanica **195**(2008), 81–102.

[29] Sengoz K.: *Development of A Generalized Isotropic Yield Surface for Pressure Insensitive Metal Plasticity Considering Yield Strength Differential Effect in Tension, Compression and Shear Stress States.* Phd thesis, George Washington University, Washington DC 2017.

[30] Zyczkowski M.: *Discontinuous bifurcations in the case of the Burzynski-Torre yield condition.* Acta Mech. **132**(1999), 19–35.

[31] Torre C.: *Grenzbedingungen fur sproden Bruch und plastisches Verhalden bildsamer.* Metall. Ing. Arch. **4**(1950), 174–189.

[32] Brokaw R.S.: *Viscosity of gas mixtures.* NASA Tech. Note, D-4496 1968.

[33] Hongjun Z., Zhengping Z., Yu L., Jian Y., Songhe Y.: *Conjugate heat transfer investigations of turbine vane based on transition models.* Chinese J. Aeronaut. **26**(2013), 890–897.

[34] Lin G., Kusterer K., Ayed A.H., Bohn D., Sugimoto T.: *Conjugate heat transfer analysis of convection-cooled turbine vanes using $\gamma - Re_\theta$ transition model.* IGPP **6**(2014).